Calcium Silicate/Chitosan-Coated Electrospun Poly (Lactic Acid) Fibers for Bone Tissue Engineering

Chu-Jung Su [a,1], Ming-Gene Tu [b,1], Li-Ju Wei [c], Tuan-Ti Hsu [c], Chia-Tze Kao [d,e], Tsui-Han Chen [f], Tsui-Hsien Huang [d,e*]

[a] Antai Medical Care Cooperation, Antai Tian-Sheng Memorial Hospital, Pingtung City, Taiwan

[b] School of Dentistry, China Medical University, Taichung City, Taiwan

[c] 3D Printing Medical Research Center, China Medical University Hospital, China Medical University, Taichung City, Taiwan

[d] School of Dentistry, Chung Shan Medical University, Taichung City, Taiwan

[e] Department of Stomatology, Chung Shan Medical University Hospital, Taichung City, Taiwan

[f] Institute of Oral Science, Chung Shan Medical University, Taichung City, Taiwan

1: Both authors contributed equally to this work.

Correspondence:

Tsui-Hsien Huang, School of Dentistry, Chung Shan Medical University, Taichung City, Taiwan (E-mail: thh@csmu.edu.tw)

Acknowledgements
The authors acknowledge receipt grants from Chung Shan Medical University and Antai Tian-Sheng Memorial Hospital under the project (CSMU-TSMH-105-03) and the Ministry of Science and Technology (MOST 105-2314-B-039-028). The authors declare that they have no conflicts of interest.

Keywords: *Poly (lactic acid); chitosan; calcium silicate; tissue engineering; osteogenesis*

Peer-reviewed version available at Materials 2017, 10, , 501; doi:10.3390/ma10050501

ABSTRACT

Electrospinning is the versatile technique to generate large quantities of micro- or nano-fibers from a wide variety of shapes and sizes of polymer. Natural bone is a hierarchically composites with the dispersion of inorganic ceramic along organic polymer. The aim of this study, the electrospun poly (lactic acid) (PLA) mats coated with chitosan (CH) and calcium silicate (CS) powder were fabricated. The morphology, chemical composition, and surface properties of CS/CH-PLA composites were characterized by scanning electron microscopy, X-ray diffraction, and Fourier transform infrared spectroscopy. In vitro, the CS/CH-coated PLA mats increased the formation of apatite on the surface when soaking in cell cultured medium. During culture, the adhesion and proliferation of the human mesenchymal stem cells (hMSCs) cultured on CS/CH-PLA were significantly promoted relative to those on PLA. Collagen I and fibronectin levels and promoted cell adhesion were observed upon an increase in CS content. Further, compared to PLA mats without CS/CH, CS10 and CS15 mats markedly enhanced the proliferation of hMSCs as well as their osteogenesis properties, which was characterized by bone-related gene expression. Our results demonstrated that the biodegradable and electroactive CS/CH-PLA mats had potential application as an ideal candidate for bone tissue engineering. Together, findings from this study clearly demonstrated that PLLA-C2S composite scaffold may function as an ideal candidate for bone tissue engineering.

1. Introduction

Tissue engineering has been intensively studied in the past few decades, and it aims to develop biological materials that restore, maintain, and enhance the regeneration of damaged tissues and organs [1]. Electrospinning is a versatile technique that generates large quantities of micro- or nano-fibers from composites containing inorganic materials and polymers of a wide variety of shapes and sizes [2,3]. Recent reviews have reported many studies that focus on producing electrospun nanofibers from biodegradable polymers [4], including the FDA-approved synthetic polymers such as poly glycolide (PGA), poly(ε-caprolactone) (PCL) [5], poly(lactic acid) (PLA) [2,6] and their copolymers P(LLA-CL), and PLGA [7]. Natural proteins, such as collagen, gelatin, silk, chitosan, and alginate, [8,9] and the blends of the polymers[10] mentioned previously are also applicable materials for electrospinning. Among all the biodegradable materials, the thermoplastic and biocompatible PLA is one of the most promising bio-based polymers [2,6] that can be used in textile, drug-carrier, and implant applications. More recently, PLA-based materials have been utilized in more durable applications in automotive, communication, and electronic industries. However, pure PLA is a typical hydrophobic polymer that lacks cell-recognition signals and is limited in its biomaterial applications [11].

Natural bone is a hierarchically composites with the dispersion of inorganic apatite along organic fibers [12]. Thus, the components of natural bones inspire us to design novel organic-inorganic hybrid bone substitute [13]. Chitosan (CH) is a natural polymer with positively charged that is a derivative of chitin and is obtained by the partial deacetylation of chitin with alkaline or enzymatic hydrolysis [14]. The benefits of using it

as a biomaterial, particularly for orthopaedic applications, include biocompatibility and minimal inflammatory potential, intrinsic antibacterial properties, and biodegradability [14]. However, the CH temporary scaffold supplies the required support for the tissue growth and regeneration [15,16]. The component and chemical structure of the CH is similar to the extracellular matrix of the bone and cartilage [15]. In addition, the CH-based scaffolds also demonstrated good osteoconductivity, which promotes hard tissue regeneration both in vitro and vivo [17]. However, due to the low mechanical properties of chitosan scaffold, its applications in orthopedic implant were limited [18]. Based on the physicochemical and biological properties properties of the CH/ceramics composite in bone tissue engineering is promising for structural bone repair [19,20].

Calcium silicate (CS)-based ceramics exhibit eminent biocompatibility, bioactivity and biodegradability that had been commonly used in hard tissue engineering applications [21-23]. The CS-based materials showed slow degradation, and its contained anti-bacterial behavior particularly in the early stage with potentially affect its clinical efficacy in endodontic use [24]. The hydrophilic of CS and its ability to develop apatite outer layers promote cellular attachment, proliferation, and differentiation and, therefore, making CS itself a promising biomaterial for bone tissue regeneration [25]. In previous reports show that CS-based materials are able to enhance osteogenic differentiation from various types cell, such as human mesenchymal stem cells (hMSCs), human dental pulp cells (hDPCs) and human periodontal ligament cells (hPDLs) [23,26-28]. In addition, it has been further reported that extracellular Ca ion has significant effect on osteoblast proliferation and differentiation. On the other hand, Si plays essential roles in early stages of bone tissue development and calcification [24]. These advantages of CS materials are

mainly related to the release of Ca and Si in the appliance areas that has been confirmed Si ion can promote the deposition of hard tissue such as bone and cementum [29,30].

The purpose of this study is to develop a novel composite bone substitute composed of CS/CH-coated PLA mat. The physicochemical properties of four types of CS/CH-coated PLA electrospun substrate were characterized. The CS powder was incorporated into CH coatings resulting in a simple one step coating procedure. The coated CS/CH were considered by X-ray powder diffraction (XRD) and Fourier transform infrared spectroscopy (FTIR). In addition, the efficacy in accelerating protein adsorption and short-term human mesenchymal stem cells (hMSCs) adhesion were analyzed. Finally, the adhesion, proliferation, and osteogenic differentiation of hMSCs were investigated to consider the efficacy of the surface coated.

2. Materials and methods

2.1. Fabrication of PLA nanofiber mat

PLA was constructed into nanofiber using a previously described electrospinning process with some modifications [31]. Briefly, PLA (Mn = 146,000, Nature Works LLC, Minnetonka, MN) was dissolved in a chloroform/DMSO mixture (75:25, v/v) by stirring for overnight. For the electrospinning process, the system consisted of a power supply (ES30P, Gamma High Voltage Research, USA), a syringe pump (LSP04-1A, Baoding Longer Precision Pump Co., Ltd., China), and a metal board used for collection. The resulting polymer solution (6%, w/v) was then directly electrospun onto the aluminum foil-covered collector (21 kV, 23 G injection needle, 0.5 ml/h injection rate, 18 cm distance between the needle and the collector). The polymer solution was placed in a 5-mL syringe fitted to a needle spinneret (0.17 mm). An electrospinning voltage was applied to the needle using a high-voltage power supply (Chargemaster CH50 Electrostatic Generating Power Supplies, SIMCO Industrial Static Control, Hatfield, PA).

2.2. Calcium silicate/chitosan coating

The method of the preparation of CS powder has been described below. Appropriate amounts of CaO (Showa, Tokyo, Japan), SiO_2 (High Pure Chemicals, Saitama, Japan), and 5% Al_2O_3 (Sigma-Aldrich, St Louis, MO) powders are mixed and sintered at 1400 °C for 2 h using a high-temperature furnace. Then, the powders were ball-milled in ethyl alcohol using a centrifugal ball mill (S 100, Retsch, Hann, Germany) for 6 h. The 10 g CS powder were stirred in 100 mL 0.1 N acetic acid for 12 h and washed by deionized water for three times. Then, the CS suspensions were filtered

through 0.22 μm filter paper and dried in an oven at 60°C. The chitosan solution (0.25%) was prepared dissolving 0.25 g chitosan in 100 mL 0.1N acetic acid and magnetically stirring for 1 day under room temperature. The acidulated CS powder were dissolved in chitosan solution for 1 day. The CS concentration of solution in this study were 0%, 0.05%, 0.10%, and 0.15% (referred to as CS0, CS5, CS10, and CS15, respectively). The 500 μL of CS/chitosan solution were covered on PLA mat for 3 h followed by being thoroughly rinsed with distilled water for 2 min three time and dried in an oven at 40°C.

2.3. Characterization of CS/chitosan/PLA mat

The water contact angle on each mat was analyzed at room temperature. Briefly, a met was placed on the top of a stainless steel base. A drop of deionized water (5 μL) was placed on the surface of the met, and an image was taken by a digital camera after an elapsed time of 30 s. The image was analyzed using ImageJ software (National Institutes of Health) to determine the water contact angle. The phase composition of CS/chitosan/PLA met was measured by X-ray diffractometry (XRD; Bruker D8 SSS, Karlsruhe, Germany). The operation condition was 30 kV and 30 mA at a scanning speed of 1°/min. FTIR (IRPrestige-21, Shimadzu Scientific Inc., Japan) was performed to consider the chemical group transformation, and the spectra were collected over a range of 800–2000 cm^{-1}.The specimens were coated with gold and their morphologies were investigated under a scanning electron microscope (SEM; JSM-6700F, JEOL) operated in the lower secondary electron image (LEI) mode at 3 kV accelerating voltage.

2.4. Weight loss

The degree of degradation was determined by monitoring the weight change of the specimen following immersion in Dulbecco's modified Eagle's medium (DMEM, Caisson). After drying at 40°C, the specimens were weighed both before and after immersion using a balance (TE214S, Sartorius, Goetingen, Germany). Ten specimens were examined for each of the materials investigated at each time point.

2.5. Cell adhesion and proliferation

Before performing the cell experiments, all samples were sterilized by being soaked in 75% ethanol and exposed to ultraviolet light for 30 min. The human mesenchymal stem cells (hMSCs) were obtained from Sciencell Research Laboratories (Sciencell, Carlsbad, CA) and grown in mesenchymal stem cell medium (Sciencell) at passage 3–6. The hMSCs were directly cultured on the sterilized specimens at a density of 10^4 cells per well in a 24-well plate and incubated at 37°C in a 5% CO_2 atmosphere for various numbers of days. After different culturing times, cell viability was evaluated using the PrestoBlue® (Invitrogen, Grand Island, NY) assay. At the end of the culture period, the medium was discarded and the wells were washed twice with cold PBS. Each well was filled with a 1:9 ratios of PrestoBlue® in fresh DMEM and incubated at 37°C for 60 min. The solution in each well was then transferred to a new 96-well plate and read using Tecan Infinite 200® PRO microplate reader (Tecan, Männedorf, Switzerland) at 570 nm with a reference wavelength of 600 nm. hMSCs cultured on tissue culture plates without materials were used as a control (Ctl). The results were obtained in triplicate from three separate experiments in terms of optical density (OD).

2.6. Collagen adsorption on substrates

After being cultured for different periods of time, the amounts of collagen (COL) and fibronectin (FN) secreted from cells onto the specimens' surface were analyzed using ELISA assay. The cells were detached using a trypsin-EDTA solution (Cassion) after being washed three times with cold PBS. Samples were then washed three times with PBS-T (PBS containing 0.1% TWEEN-20), followed by blocking with 5% bovine serum albumin (BSA; Gibco) in PBS-T for 1 h. Dilutions of primary antibodies were set at 1:500. Following this procedure, the mats were incubated with anti-human β-actin, anti-human COL I or anti-FN antibody (GeneTex, San Antonio, TX) for 2 h and shaken under 25 rpm at room temperature. Afterwards, specimens were washed three times with PBS-T for 5 min and incubated with horseradish peroxidase (HRP)-conjugated secondary antibodies for 1 h at room temperature with shaking. The samples were then washed three times with PBS-T for 10 min each and then One-Step Ultra TMB substrate (Invitrogen) was added to the wells and developed for 30 min at room temperature in the dark, after which an equal volume of 2M H_2SO_4 was added to stop and stabilize the oxidation reaction. The colored products were then transferred to new 96-well plates and read using a multiwell spectrophotometer at 450 nm with reference at 620 nm, according to the manufacturer's recommendations. All experiments were carried out in triplicate. Additionally, β-actin antibodies were used as a control.

2.7. Cell morphology

After the cells cultured on met for 3 h and 1 day, the specimens were washed three times with cold PBS and fixed in 1.5% glutaraldehyde (Sigma) for 2 h, after which they were dehydrated using a graded ethanol series for 20 min at each concentration and dried with liquid CO_2 using a critical point dryer device (LADD 28000; LADD, Williston, VT). The dried specimens were then mounted on stubs, coated with gold, and viewed using scanning electron microscopes (JEOL JSM-7401F, Tokyo, Japan). For immunofluorescent staining, cells were seeded on substrates for 3 and 7 days. Cells were fixed by 4% paraformaldehyde for 30 min and permeabilized by 0.1% Triton X-100 for 15 min. Then, specimens were blocked with 2% BSA for 1 h. These cells were incubated with AlexaFluor-488-conjugated phalloidin (green color) for 1 h at room temperature. The specimens were then washed with TBS-T thrice and the cells were photographed under indirect immunofluorescence using a Zeiss Axioskop 2 microscope (Carl Zeiss, Thornwood, NY).

2.8. Real-time PCR

For the detection of bone-related gene [collagen I (COL), alkaline phosphatase (ALP), osteopontin (OPN), and osteocalcin (OC)] of hMSCs, which were cultured at a density of 10^4 cells per sample for different time-points (3 and 7 days). Total RNA of all groups was extracted using TRIzol reagent (Invitrogen) and analyzed by RT- qPCR. Total RNA (500 ng) was used for the synthesis of complementary DNA using cDNA Synthesis Kit (GenedireX) following the manufacturer's instructions. RT-qPCR primers (Table 2) were designed based on cDNA sequences from the NCBI Sequence database.

SYBR Green qPCR Master Mix (Invitrogen) was used for detection and the target mRNA expressions were assayed on the ABI Step One Plus real-time PCR system (Applied Biosystems, Foster City, California, USA). Each sample was performed in triplicate.

2.9. Statistical Analysis

A one-way analysis of variance statistical analysis was used to evaluate the significance of the differences between the means in the measured data. Scheffe's multiple comparison test was used to determine the significance of the deviations in the data for each specimen. In all cases, the results were considered statistically significant with p value < 0.05.

3. Results and discussion

3.1. Characterization of CS/CH/PLA

The hydrophilic properties of the pure PLA and CS/CH-coated PLA mat were tested by measuring the contact angle as shown in Fig. 1. High contact angle (>100o) of pure PLA and HA-coated (CS0) mat specimens were observed when comparing to CH/HA-coated PLA specimens. There is no significant effect on the hydrophilicity of the PLA mats with CH coating. The contact angle of prepared CS/CH-coated PLA mat specimens could be decreased from 91.2 ± 3.8º, 79.3 ± 3.2º and 35.1 ± 2.1º with increasing CS coating concentration by 0.05% CS (CS5), 0.1% CS (CS10), and 0.15% CS (CS15), respectively. The higher content of CS coating, the higher hydrophilic properties of the mat specimens were measured. The result show that CS0 scaffold is hydrophobic, while the mat coated with CS powder precipitate are extremely hydrophilic, that the cell behavior can be affected if grown on specimens with a water contact angle in this range [32].

Fig. 2 shows the XRD patterns of the CS/CH-coated PLA mat. There were no mineral-related peaks were observed for the PLA and CS0. More identical peaks can be examined in CS-contained specimens (CS10 and CS15), when compared with CS5. The main peaks at around 2θ = 29.4° and 2θ = 39.2° are characteristic of CS [33]. As can be seen, peak intensity increased when CS concentration increased in CH coated on the surface of the PLA mat.

The characteristic peaks of PLA and CS/CH-coated PLA mats measured from FTIR spectra are shown in Fig. 3. The spectra of PLA produced intense absorbance at 1750 cm^{-1}, 1100 cm^{-1} due to C=O and C-O stretch. The chitosan was substantiated by the bands in

the 1585 cm^{-1} and 1655 cm^{-1} regions related to NH_2 scissoring and C=O stretching peaks, respectively. The broad peaks at 1010 cm^{-1} and 1051 cm^{-1} were assigned to the C–O stretching vibration in chitosan. As increasing the CS concentration during coating process, the two peaks became less evident. A broadest peak from 1000 to 1350 cm^{-1} corresponded to Si-O and Si-O-Si stretch resulted from increasing content which shown in specimen CS15.

3.2. Bioactivity

Fig. 4 shows the SEM images of the PLA and CS/CH-coated mat samples. After immersion in DMEM for 7 day, there were no apatite precipitation on the PLA and CS0 samples. Evidently, increasing CS contained induced more apatite precipitation on the surface of the composites, which is in good agreement with the SEM results. As for the CS15 specimen, the development of large quantities of apatite were observed which formed a thick outer layer on the PLA mats. The Si–OH functional groups on the surface of CS materials have been proven to act as nucleation center for apatite precipitation [24]. The apatite precipitated on specimens in DMEM has verified to be useful in predicting the materials-bone binding force in vitro.

The concentrations of Ca, Si and P ion release in various immersion time periods in DMEM are shown in Fig. 5. The CS/CH coated PLA mats effected the Ca ion concentration release rates. The Ca ion release rates increased with increasing CS coating content after the first day of immersion and the concentration gradually decreased to below 1.0 mM. The Ca ion release rate decrease since the immersion commenced to the PLA specimens without CS coating. However, the higher initial content of the CS coating,

the lower final Ca concentration was measured as shown in Fig 5A. The higher CS coating content, the higher Si concentration and the lower P concentration. The amount of Si that was released from each of the specimens was presented in Fig 5B. Si is continuously released during the soaking from 1 to 14 days, indicating that the CS15 are slowly released Si ion over the entire period of the immersion process. After CS0, CS5, CS10, and CS15 soaked in DMEM for 14 days, Si ion concentration of solution was 0, 0.71, 1.12, and 1.52 mM, respectively. Several studies provided the CS-contained materials not only with excellent bioactivity [23], but also promoted cementogenesis and angiogenesis of primary cells [34]. In contrast, P ion significantly declined at the groups contained CS for all immersion time-points (Fig. 5C). The results demonstrated that CS15 with a optimum bioactivity was expected to form a chemical bond between bone substitutes and hard tissue through the thickness apatite layer.

Biodegradation rate of a biomaterial can be justified by the its weight loss through dissolubility in DMEM solution. Fig. 6 shows the weight loss of each specimen after immersion in DMEM solution from 1 week to 12 weeks. All specimens showed higher weight loss rate during the first 2 weeks of soaking and turn moderate. The PLA shows much less degradation than the other membranes, exhibiting a weight loss of 5.38% after immersion in the DMEM for 4 weeks. The CH and CH/CS coated PLA mat specimens showed higher degradation rate when compared to PLA mat specimens. CS15 showed the highest degradation rate among all specimens and the weight loss reached to 22.01% after 8 weeks. At the final time-point of the soaking, weight losses of approximately 8.12%, 16.82%, 19.01%, 22.51%, and 25.41% were observed for the PLA, CS0, CS5, CS10, and

CS15 mats, respectively, indicating significant differences ($P < 0.05$). It is well known that biomaterials with various degradation rates are required in different clinical use [25].

3.3. Protein adsorption

The effect of CS/CH-coated on the adsorption of Col I and FN by cells was also examined. Col I adsorption was significantly ($p < 0.05$) higher on the specimens with the highest CS-contained (CS15) than on the PLA mat after cell seeding for 3 h (Fig. 7). The percentage increase in the Col I secretion was 51%, 79% and 117% for CS5, CS10, and CS15 respectively, compared with CS0. In CS-contained groups, the pH was reduced around the micro-environment and caused the collagen assemble on the specimen surface [35]. The covalent immobilization of COL I on the material surface was promoted the uniformity and stability of the COL I adsorption on specimens [36]. The Si–OH groups and silicate not only supplied active sites for nucleation of hydroxyapatite, but also contributed to their cell behavior, such as adhesion and proliferation [37]. COL I is the most abundant proteins in nature bone, are defined by a characteristic triple helix structure with a repetitive amino acid and interacted with various biomolecules mediated cell adhesion and affected cell function [38,39]. Following initial spreading, the COL I or FN on the substrate, which regulated cell adhesion-related protein and the induction of signaling pathways that are required for cell motility [40].

3.4. Cell adhesion and proliferation

The facilitation of cell adhesion on the CS/CH-coated PLA was confirmed and observed by SEM (Fig. 8). When the cells were cultured onto PLA specimen for 3 h, the

cells barely adhered and spread, whereas the cells cultured on CS-contained samples were showed normal adhesion. Cell adhesion requires the presence of a suitable proteinaceous substrate to which cell adhesion receptors, such as integrins, can adhere and form cell-anchoring points. The dominating role of protein adsorption in the effect of cell adhesion has been identified [40]. Fig. 9 indicated the cell adhesion and proliferation of hMSCs cultured on various specimens for different time-points. Fig. 9A shows that more cells adhered to the CS15 compared with PLA and CS0 after 3 and 12 h. For example, after 3 h of cultured, percentage increase in the cell attachment was 25.1%, 39.7% and 46.6% for CS5, CS10 and CS15, respectively, compared with CS0. The cell proliferation gradually increased with increasing amount of CS on CH, which indicated a significant difference ($p < 0.05$) compared with the PLA mats. The CS15 elucidated an increase of approximately 31.3% in the OD value referenced to the CS0. In addition, Fig. 10 shows the immunofluorescence images of hMSCs stained by FITC on the mats, which displayed limpid F-actin after cultured for 3 and 7 days. Most of the hMSCs are stained in green, and they display typically polygonal morphologies after 3 days. They kept growing on both types of scaffolds until cell were formed upon 7 days of culture. Also, it was clear that the cells on CS15 scaffolds were larger than those on PLA and CS0. In this study, it was found that the Si ions released from the CS-contained specimens, and the Si ion concentrations were almost similar to the values previously reported that enhanced cell function [41]. Therefore, it can be considered that the Si ions with certain concentration released from the CS/CH-PLA composite mats enhanced the proliferation of hMSCs. Wu et al. found similar results for low concentrations of CS-contained composites in proliferation of human osteoblast cells [42].

3.5. Osteogenesis gene expression

The PLA mat acted as a control to evaluate the effect of the coated with CS/CH on the expression of the osteogenic-related gene. There is no obvious difference for the COL gene expression between all specimens at day 7 and 14 (Fig. 11A). According to the results shown in Fig. 11, CS0 did not generate any stimuli on the specific ALP gene expression compared to the PLA. CS15 and CS20 were generated higher specific ALP expression than PLA for all time point. Among other groups, CS15 showed the highest level for all genes particularly at day 14; the stimulation was as high as 1.7-, 1.3-, and 1.4-fold, for ALP, OPN, and OC, respectively, with respect to CS0. ALP is an early marker of osteogenesis differentiation, and it is generally accepted that an increase in the specific activity of ALP in bone cells reflects a shift to a more differentiated state [43]. OPN and OC are later makers of osteogenic differentiation. The CS-contained specimens significantly promoted the osteogenesis-related gene expression (ALP, OCN and OC) of hMSCs compared with the CH-coated PLA group. The positive effects of Si on the osteogenic differentiation of hMSCs and osteoblast cells have been proved by various studies [43,44]. In the present work, a sustained release of Si ions was observed from the CS/CH-coated PLA, which might account for the promoted osteogenesis differentiation of hMSCs cultured on the CS/CH-coated PLA mats. Wu et al. showed that CS-based biomaterials could promote the osteogenesis differentiation and calcium deposition of human dental pulp cells and in vivo bone regeneration [45].

4. Conclusions

In this study, we fabricated PLA mat via electrospinning, which were coated with CH/CS as a simple surface modification. SEM shows homogeneously CS/CH-coated on the PLA mats that indicated the CS15 showed better capability to increase apatite particulates deposition when immersed in DMEM. From the study with hMSCs, we confirmed that the COL I and FN adsorption, cell adhesion, and proliferation were significantly increased on CS15 specimens. In vitro hMSCs cultivation on pure PLA and CS/CH-containing mats proven that the addition of the inorganic component did not lead to toxicity whereas it enabled promoted cell attachment, proliferation, leading to significantly increased osteogenesis. Our results prove that simple surface coating on the bioactive and biodegradable fiber substrates using CS/CH is a very promising tool to affect stem cell behavior, which may appear to be a promising candidate for bone tissue engineering.

.

Acknowledgements

The authors acknowledge receipt grants from Chung Shan Medical University and Antai Tian-Sheng Memorial Hospital under the project (CSMU-TSMH-105-03) and the Ministry of Science and Technology (MOST 105-2314-B-039-028). The authors declare that they have no conflicts of interest.

References

1. Mikos, A.; Herring, S.; Ochareon, P. Engineering complex tissues. *Tissue Eng* **2006**, *12*, 3307–3339.
2. Lin, C. C.; Fu, S. J.; Lin, Y. C.; Yang, I. K.; Gu, Y. Chitosan-coated electrospun PLA fibers for rapid mineralization of calcium phosphate. *Int J Biol Macromol* **2014**, *68*, 39–47.
3. Song, B.; Wu, C.; Chang, J. Dual drug release from electrospun poly(lactic-co-glycolic acid)/mesoporous silica nanoparticles composite mats with distinct release profiles. *Acta Biomater* **2012**, *8*, 1901–1907.
4. Dong, Y.; Liao, S.; Ngiam, M.; Chan, C. K.; Ramakrishna, S. Degradation behaviors of electrospun resorbable polyester nanofibers. *Tissue Eng Part B Rev* **2009**, *15*, 333–351.
5. Holzwarth, J. M.; Ma, P. X. Biomimetic nanofibrous scaffolds for bone tissue engineering. *Biomaterials* **2011**, *32*, 9622–9629.
6. Yang, F.; Murugan, R.; Wang, S.; Ramakrishna, S. Electrospinning of nano/micro scale poly(L-lactic acid) aligned fibers and their potential in neural tissue engineering. *Biomaterials* **2005**, *26*, 2603–2610.
7. Li, M.; Liu, W.; Sun, J.; Xianyu, Y.; Wang, J.; Zhang, W.; Zheng, W.; Huang, D.; Di, S.; Long, Y.-Z.; Jiang, X. Culturing primary human osteoblasts on electrospun poly(lactic-co-glycolic acid) and poly(lactic-co-glycolic acid)/nanohydroxyapatite scaffolds for bone tissue engineering. *ACS Appl Mater Interfaces* **2013**, *5*, 5921–5926.
8. Sun, X.; Cheng, L.; Zhao, J.; Jin, R.; Sun, B.; Shi, Y.; Zhang, L.; Zhang, Y.; Cui, W. bFGF-grafted electrospun fibrous scaffolds via poly(dopamine) for skin wound healing. *J Mater Chem B* **2014**, *2*, 3636–3645.
9. Rajzer, I.; Menaszek, E.; Kwiatkowski, R.; Planell, J. A.; Castaño, O. Electrospun gelatin/poly(ε-caprolactone) fibrous scaffold modified with calcium phosphate for bone tissue engineering. *Mater Sci Eng C Mater Biol Appl* **2014**, *44*, 183–109.
10. Gunn, J.; Zhang, M. Polyblend nanofibers for biomedical applications: perspectives and challenges. *Trends Biotech* **2010**, *28*, 189–197.
11. Kai, D.; Liow, S. S.; Loh, X. J. Biodegradable polymers for electrospinning: Towards biomedical applications. *Mater Sci Eng C Mater Biol Appl* **2014**, *45*, 659–670.
12. Wang, C.; Wang, M. Electrospun multicomponent and multifunctional nanofibrous bone tissue engineering scaffolds. *J Mater Chem B* **2017**, *5*, 1388–1399.
13. Shao, W.; He, J.; Sang, F.; Ding, B.; Chen, L.; Cui, S.; Li, K.; Han, Q.; Tan, W. Coaxial electrospun aligned tussah silk fibroin nanostructured fiber scaffolds embedded with hydroxyapatite–tussah silk fibroin nanoparticles for bone tissue engineering. *Mater Sci Eng C Mater Biol Appl* **2016**, *58*, 342–351.
14. Chen, Y.; Zhou, Y.; Yang, S.; Li, J. J.; Li, X.; Ma, Y.; Hou, Y.; Jiang, N.; Xu, C.; Zhang, S.; Zeng, R.; Tu, M.; Yu, B. Novel bone substitute composed of chitosan and strontium-doped α-calcium sulfate hemihydrate: Fabrication, characterisation and evaluation of biocompatibility. *Mater Sci Eng C Mater Biol Appl* **2016**, *66*, 84–91.
15. Kim, S.; Cui, Z.-K.; Fan, J.; Fartash, A.; Aghaloo, T. L.; Lee, M. Photocrosslinkable chitosan hydrogels functionalized with the RGD peptide and phosphoserine to enhance osteogenesis. *J Mater Chem B* **2016**, *4*, 5289–5298.

16. Yao, Q.; Li, W.; Yu, S.; Ma, L.; Jin, D.; Boccaccini, A. R.; Liu, Y. Multifunctional chitosan/polyvinyl pyrrolidone/45S5 Bioglass® scaffolds for MC3T3-E1 cell stimulation and drug release. *Mater Sci Eng C Mater Biol Appl* **2015**, *56*, 473–480.
17. Arunkumar, P.; Indulekha, S.; Vijayalakshmi, S.; Srivastava, R. Poly (caprolactone) microparticles and chitosan thermogels based injectable formulation of etoricoxib for the potential treatment of osteoarthritis. *Mater Sci Eng C Mater Biol Appl* **2016**, *61*, 534–544.
18. Guo, M.; Li, X. Development of porous Ti6Al4V/chitosan sponge composite scaffold for orthopedic applications. *Mater Sci Eng C Mater Biol Appl* **2016**, *58*, 1177–1181.
19. Guo, Y. P.; Guan, J. J.; Yang, J.; Wang, Y.; Zhang, C. Q.; Ke, Q. F. Hybrid nanostructured hydroxyapatite–chitosan composite scaffold: bioinspired fabrication, mechanical properties and biological properties. *J Mater Chem B* **2015**, *3*, 4679–4689.
20. Lei, Y.; Xu, Z.; Ke, Q.; Yin, W.; Chen, Y.; Zhang, C.; Guo, Y. Strontium hydroxyapatite/chitosan nanohybrid scaffolds with enhanced osteoinductivity for bone tissue engineering. *Mater Sci Eng C Mater Biol Appl* **2017**, *72*, 134–142.
21. Zhang, L.; Huang, X.; Han, Y. Formation mechanism and cytocompatibility of nano-shaped calcium silicate hydrate/calcium titanium silicate/TiO2 composite coatings on titanium. *J Mater Chem B* **2016**, *4*, 6734–6745.
22. Costa, F.; Sousa Gomes, P.; Fernandes, M. H. Osteogenic and angiogenic response to calcium silicate-based endodontic sealers. *J Endod* **2016**, *42*, 113–119.
23. Chen, Y. W.; Hsu, T. T.; Wang, K.; Shie, M. Y. Preparation of the fast setting and degrading Ca-Si-Mg cement with both odontogenesis and angiogenesis differentiation of human periodontal ligament cells. *Mater Sci Eng C Mater Biol Appl* **2016**, *60*, 374–383.
24. Huang, M. H.; Shen, Y. F.; Hsu, T. T.; Huang, T. H.; Shie, M. Y. Physical characteristics, antimicrobial and odontogenesis potentials of calcium silicate cement containing hinokitiol. *Mater Sci Eng C Mater Biol Appl* **2016**, *65*, 1–8.
25. Shie, M. Y.; Chiang, W. H.; Chen, I. W. P.; Liu, W. Y.; Chen, Y. W. Synergistic acceleration in the osteogenic and angiogenic differentiation of human mesenchymal stem cells by calcium silicate–graphene composites. *Mater Sci Eng C Mater Biol Appl* **2017**, *73*, 726–735.
26. Chang, N. J.; Chen, Y. W.; Shieh, D. E.; Fang, H. Y.; Shie, M. Y. The effects of injectable calcium silicate-based composites with the Chinese herb on an osteogenic accelerator in vitro. *Biomed Mater* **2015**, *10*, 055004.
27. Hsu, T. T.; Kao, C. T.; Chen, Y. W.; Huang, T. H.; Yang, J. J.; Shie, M. Y. The synergistic effects of CO2 laser treatment with calcium silicate cement of antibacterial, osteogenesis and cementogenesis efficacy. *Laser Phys Lett* **2015**, *12*, 055602.
28. Huang, C. Y.; Huang, T. H.; Kao, C. T.; Wu, Y. H.; Chen, W. C.; Shie, M. Y. Mesoporous calcium silicate nanoparticles with drug delivery and odontogenesis properties. *J Endod* **2017**, *43*, 69–76.
29. Shie, M. Y.; Ding, S. J.; Chang, H. C. The role of silicon in osteoblast-like cell proliferation and apoptosis. *Acta Biomater* **2011**, *7*, 2604–2614.
30. Chen, Y. W.; Ho, C. C.; Huang, T. H.; Hsu, T. T.; Shie, M. Y. The ionic products from mineral trioxide aggregate–induced odontogenic differentiation of dental pulp cells via activation of the Wnt/β-catenin signaling pathway. *J Endod* **2016**, *42*, 1062–1069.
31. Lin, C. C.; Fu, S. J. Osteogenesis of human adipose-derived stem cells on poly(dopamine)-coated electrospun poly(lactic acid) fiber mats. *Mater Sci Eng C Mater Biol Appl* **2016**, *58*, 254–263.

32. Cheng, Y. L.; Chen, Y. W.; Wang, K.; Shie, M. Y. Enhanced adhesion and differentiation of human mesenchymal stem cell inside apatite-mineralized/poly(dopamine)-coated poly(ε-caprolactone) scaffolds by stereolithography. *J Mater Chem B* **2016**, *4*, 6307–6315.
33. Tsai, K. Y.; Lin, H. Y.; Chen, Y. W.; Lin, C. Y.; Hsu, T. T.; Kao, C. T. Laser sintered magnesium-calcium silicate/poly-ε-caprolactone scaffold for bone tissue ngineering. *Materials* **2017**, *10*, 65.
34. Chen, Y. W.; Yeh, C. H.; Shie, M. Y. Stimulatory effects of the fast setting and degradable Ca–Si–Mg cement on both cementogenesis and angiogenesis differentiation of human periodontal ligament cells. *J Mater Chem B* **2015**, *3*, 7099–7108.
35. Pawelec, K. M.; Shepherd, J.; Jugdaohsingh, R.; Best, S. M.; Cameron, R. E.; Brooks, R. A. Collagen scaffolds as a tool for understanding the biological effect of silicates. *Mater Lett* **2015**, *157*, 176–179.
36. Yu, X.; Walsh, J.; Wei, M. Covalent immobilization of collagen on titanium through polydopamine coating to improve cellular performances of MC3T3-E1 cells. *RSC Adv* **2013**, *4*, 7185–7192.
37. Chen, S.; Osaka, A.; Ikoma, T.; Morita, H.; Li, J.; Takeguchi, M.; Hanagata, N. Fabrication, microstructure, and BMP-2 delivery of novel biodegradable and biocompatible silicate-collagen hybrid fibril sheets. *J Mater Chem* **2011**, *21*, 10942–10948.
38. Sun, X.; Fan, J.; Ye, W.; Zhang, H.; Cong, Y.; Xiao, J. A highly specific graphene platform for sensing collagen triple helix. *J Mater Chem B* **2016**, *4*, 1064–1069.
39. Lode, A.; Meyer, M.; Brüggemeier, S.; Paul, B.; Baltzer, H.; Schröpfer, M.; Winkelmann, C.; Sonntag, F.; Gelinsky, M. Additive manufacturing of collagen scaffolds by three-dimensional plotting of highly viscous dispersions. *Biofabrication* **2016**, *8*, 015015.
40. Shie, M. Y.; Ding, S. J. Integrin binding and MAPK signal pathways in primary cell responses to surface chemistry of calcium silicate cements. *Biomaterials* **2013**, *34*, 6589–6606.
41. Lai, W. Y.; Chen, Y. W.; Kao, C. T.; Hsu, T. T.; Huang, T. H.; Shie, M. Y. Human dental pulp cells responses to apatite precipitation from dicalcium silicates. *Materials* **2015**, *8*, 4491–4504.
42. Wu, Z.; Zheng, K.; Zhang, J.; Tang, T.; Guo, H.; Boccaccini, A. R.; Wei, J. Effects of magnesium silicate on the mechanical properties, biocompatibility, bioactivity, degradability, and osteogenesis of poly(butylene succinate)-based composite scaffolds for bone repair. *J Mater Chem B* **2016**, *4*, 7974–7988.
43. Liu, C. H.; Hung, C. J.; Huang, T. H.; Lin, C. C.; Kao, C. T.; Shie, M. Y. Odontogenic differentiation of human dental pulp cells by calcium silicate materials stimulating via FGFR/ERK signaling pathway. *Mater Sci Eng C Mater Biol Appl* **2014**, *43*, 359–366.
44. Hung, C. J.; Hsu, H. I.; Lin, C. C.; Huang, T. H.; Wu, B. C.; Kao, C. T.; Shie, M. Y. The role of integrin αv in proliferation and differentiation of human dental pulp cell response to calcium silicate cement. *J Endod* **2014**, *40*, 1802–1809.
45. Wu, B. C.; Kao, C. T.; Huang, T. H.; Hung, C. J.; Shie, M. Y.; Chung, H. Y. Effect of verapamil, a calcium channel blocker, on the odontogenic activity of human dental pulp cells cultured with silicate-based materials. *J Endod* **2014**, *40*, 1105–1111.

46. Shie, M. Y.; Chang, H. C.; Ding, S. J. Effects of altering the Si/Ca molar ratio of a calcium silicate cement on in vitro cell attachment. *Int Endod J* **2012**, *45*, 337–345.
47. Chien, C. Y.; Tsai, W. B. Poly(dopamine)-assisted immobilization of Arg-Gly-Asp peptides, hydroxyapatite, and bone morphogenic protein-2 on titanium to improve the osteogenesis of bone marrow stem cells. *ACS Appl Mater Interfaces* **2013**, *5*, 6975–6983.
48. Chien, C. Y.; Liu, T. Y.; Kuo, W. H.; Wang, M. J.; Tsai, W. B. Dopamine-assisted immobilization of hydroxyapatite nanoparticles and RGD peptides to improve the osteoconductivity of titanium. *J Biomed Mater Res Part A* **2013**, *101*, 740–747.
49. Rim, N. G.; Kim, S. J.; Shin, Y. M.; Jun, I.; Lim, D. W.; Park, J. H.; Shin, H. Mussel-inspired surface modification of poly(L-lactide) electrospun fibers for modulation of osteogenic differentiation of human mesenchymal stem cells. *Colloids Surf B* **2012**, *91*, 189–197.
50. Shi, X.; Li, L.; Ostrovidov, S.; Shu, Y.; Khademhosseini, A.; Wu, H. Stretchable and micropatterned membrane for osteogenic differentation of stem cells. *ACS Appl Mater Interfaces* **2014**, *6*, 11915–11923.

Figure Legends

Figure 1. Water contact angle of different various CS/CH-coated PLA mats.

Figure 2. XRD patterns of CS/CH-coated PLA mats, and the marker indicated the calcium silicate.

Figure 3. Fourier transform infrared spectra survey of various specimens.

Figure 4. Surface SEM images of the specimens before and after immersion in DMEM.

Figure 5. (A) Ca, (B) Si, and (C) P ions concentration of DMEM after specimens soaking for different times.

Figure 6. The weight loss of CS/CH-coated PLA mats immersed in DMEM for different time-points.

Figure 7. COL I and FN adsorbed on CS/CH-coated PLA mats surface by hMSCs secretion for 3 h. "*" indicates a significant difference ($p < 0.05$) compared to CS0.

Figure 8. SEM images of hMSCs adhered on CS/CH-coated PLA mats for 3 h and 1 day.

Figure 9. (A) Adhesion and (B) proliferation of hMSCs cultured on CS/CH-coated PLA mats for different time points. "*" indicates a significant difference ($p < 0.05$) compared to CS0.

Figure 10. The immunofluorescence of hMSCs cultured on CS/CH-coated PLA mats for 3 and 7 days.

Figure 11. (A) COL, (B) ALP, (C) OPN and (D) OC gene expression in the hMSCs were cultured on CS/CH-coated PLA mats for 7 and 14 days. "*" indicates a significant difference ($p < 0.05$) compared to specimen without CS0.

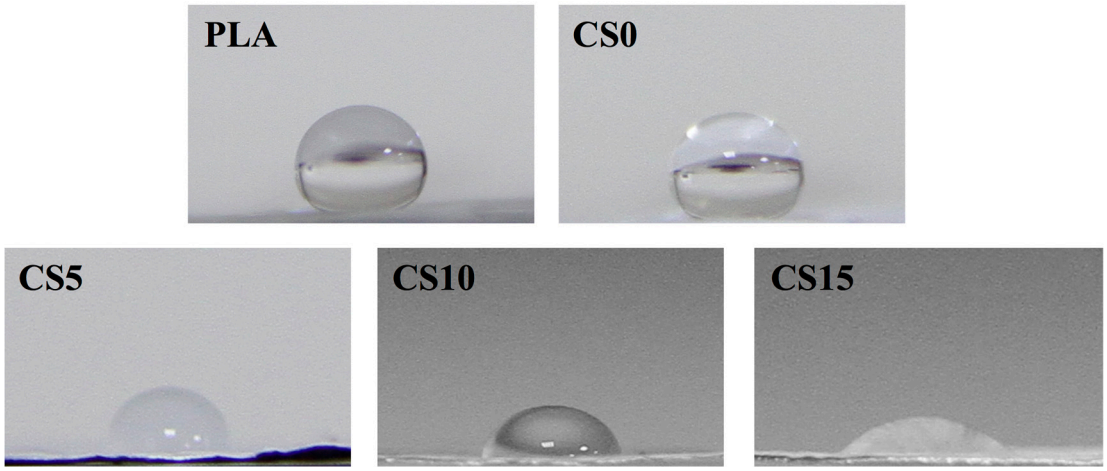

Fig. 1

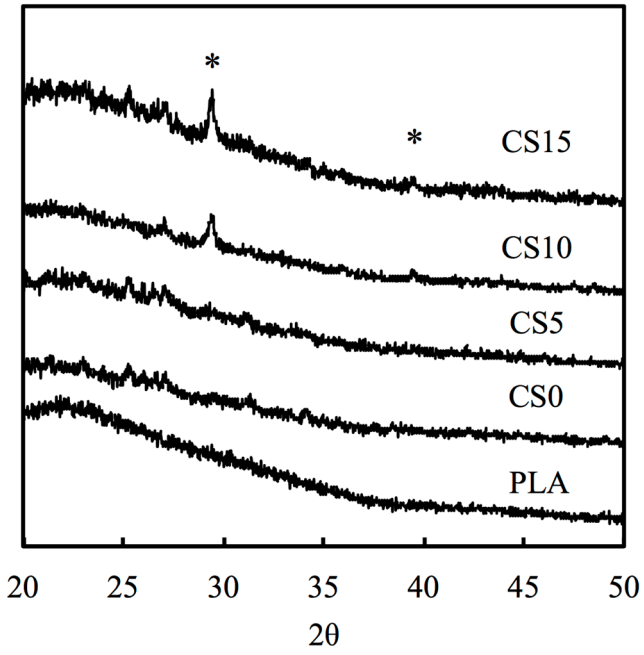

Fig. 2

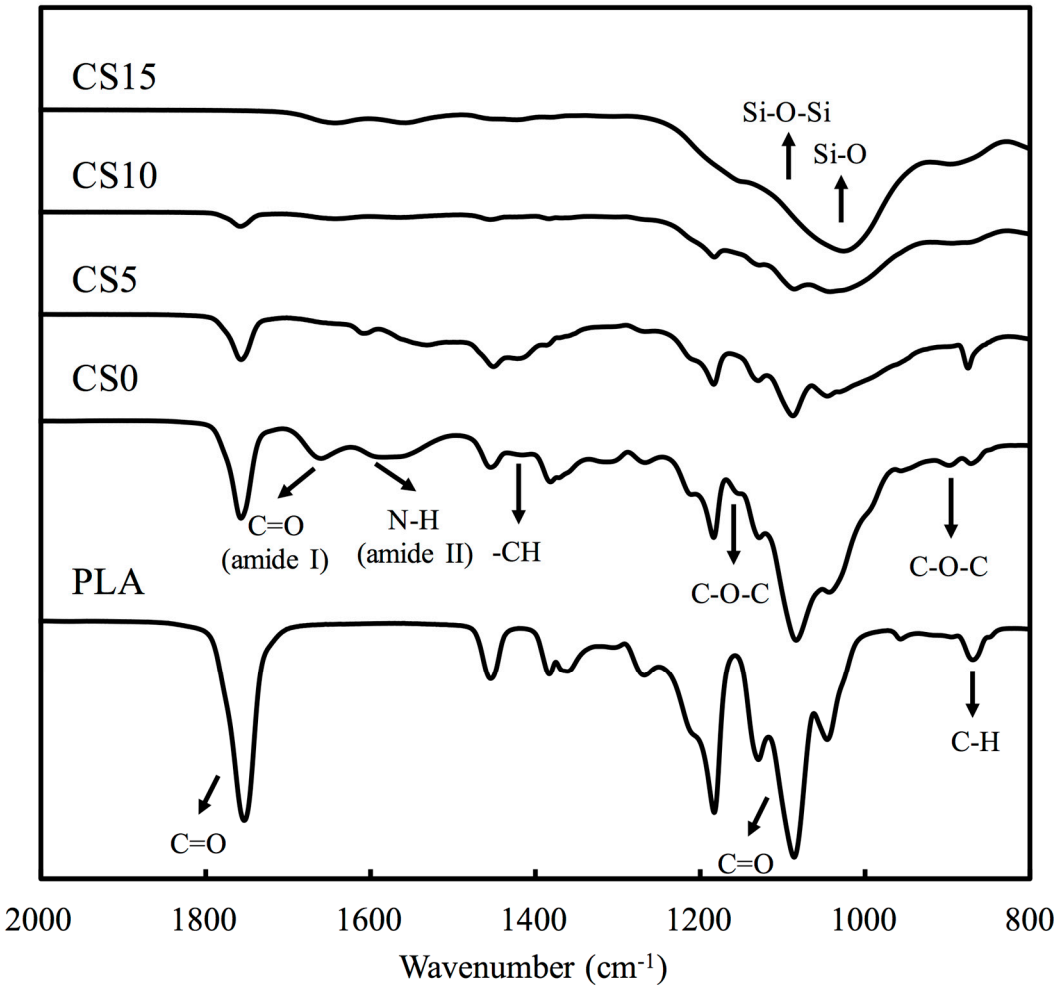

Fig. 3

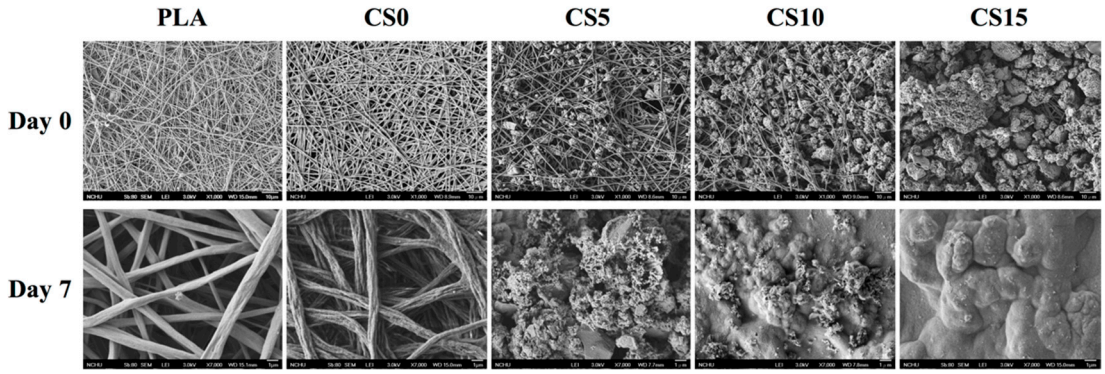

Fig. 4

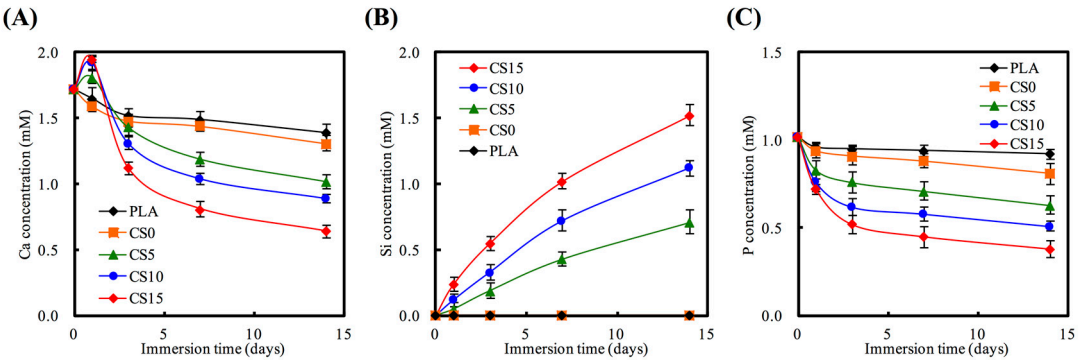

Fig. 5

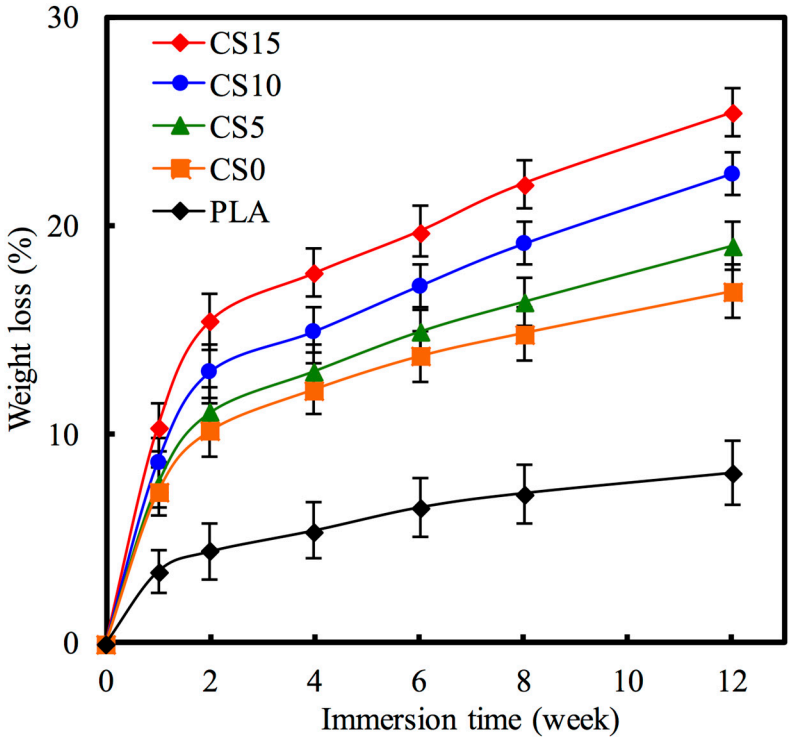

Fig. 6

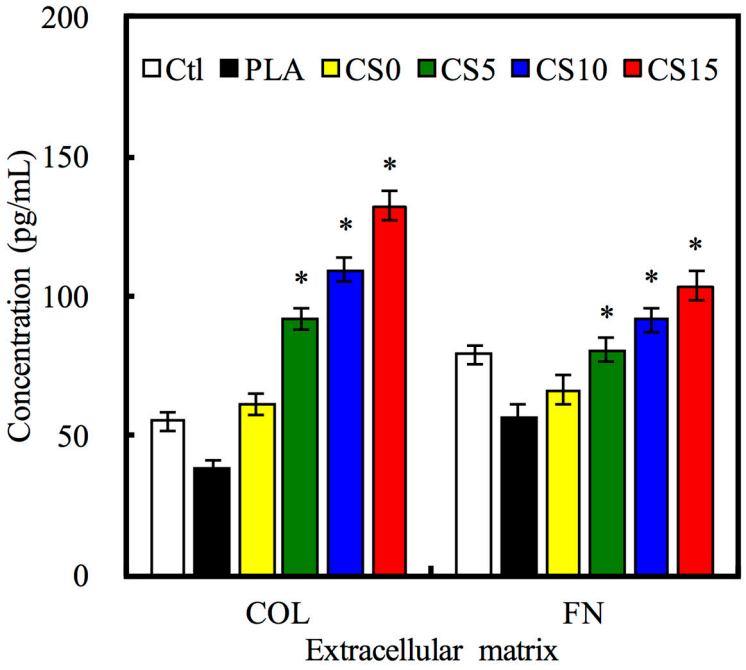

Fig. 7

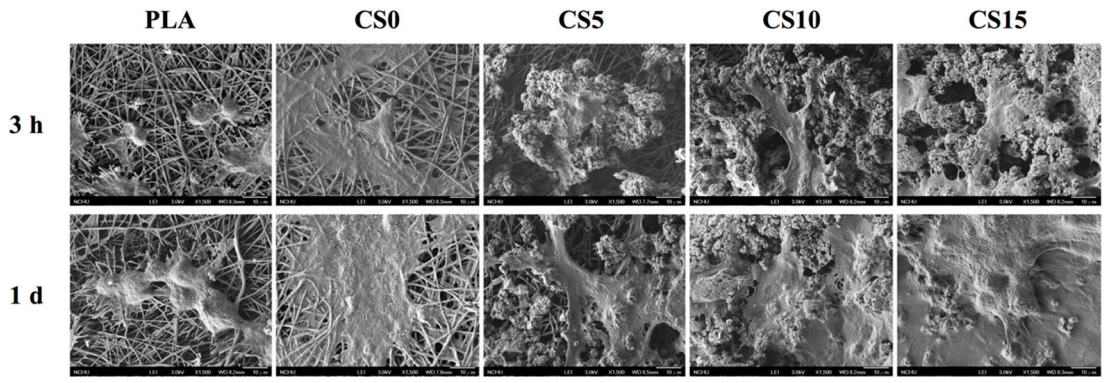

Fig. 8

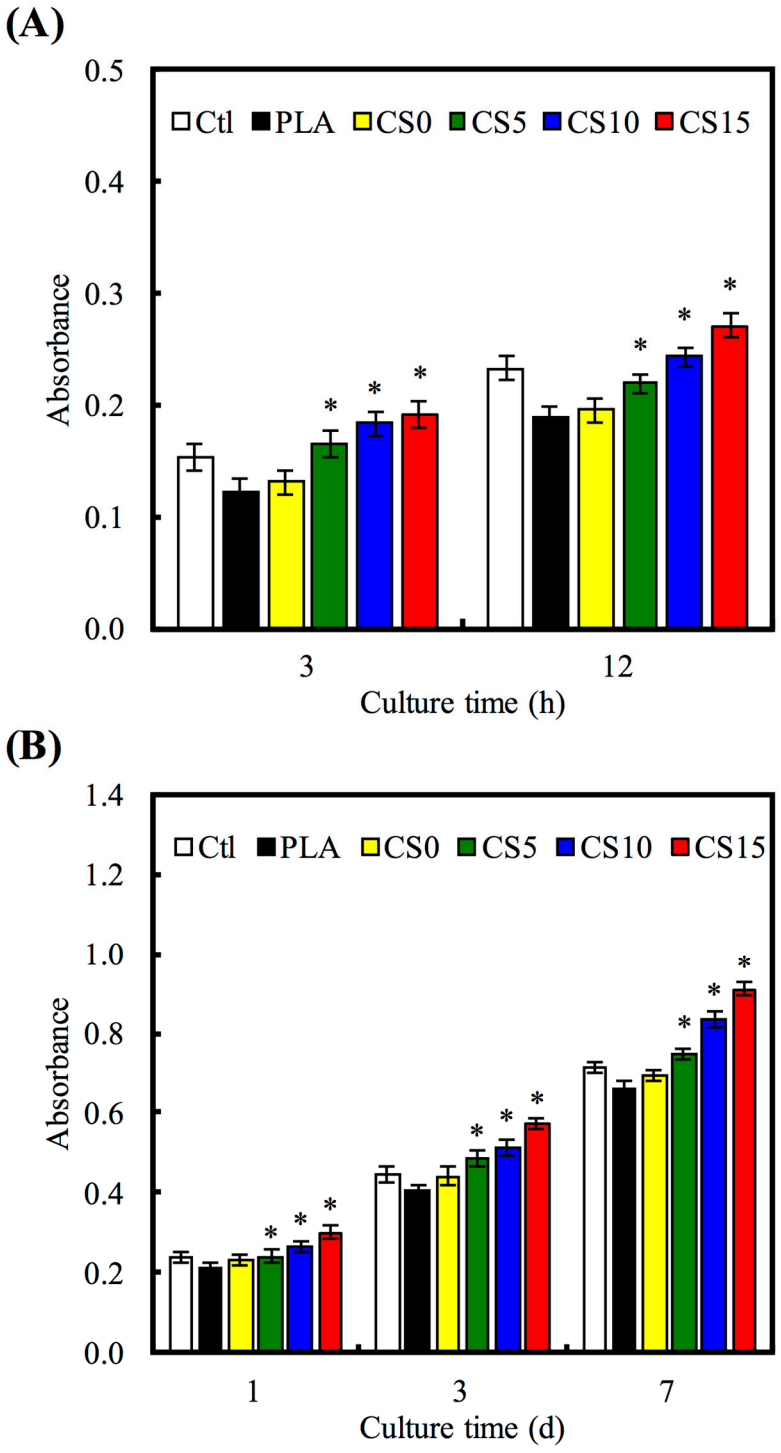

Fig. 9

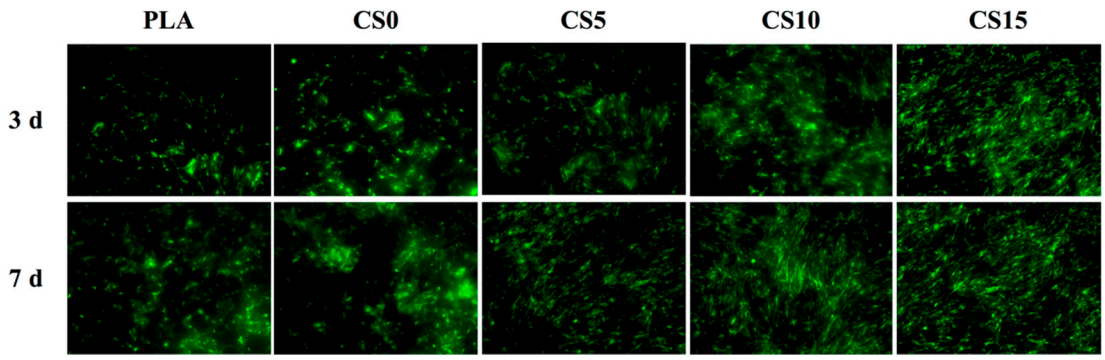

Fig. 10

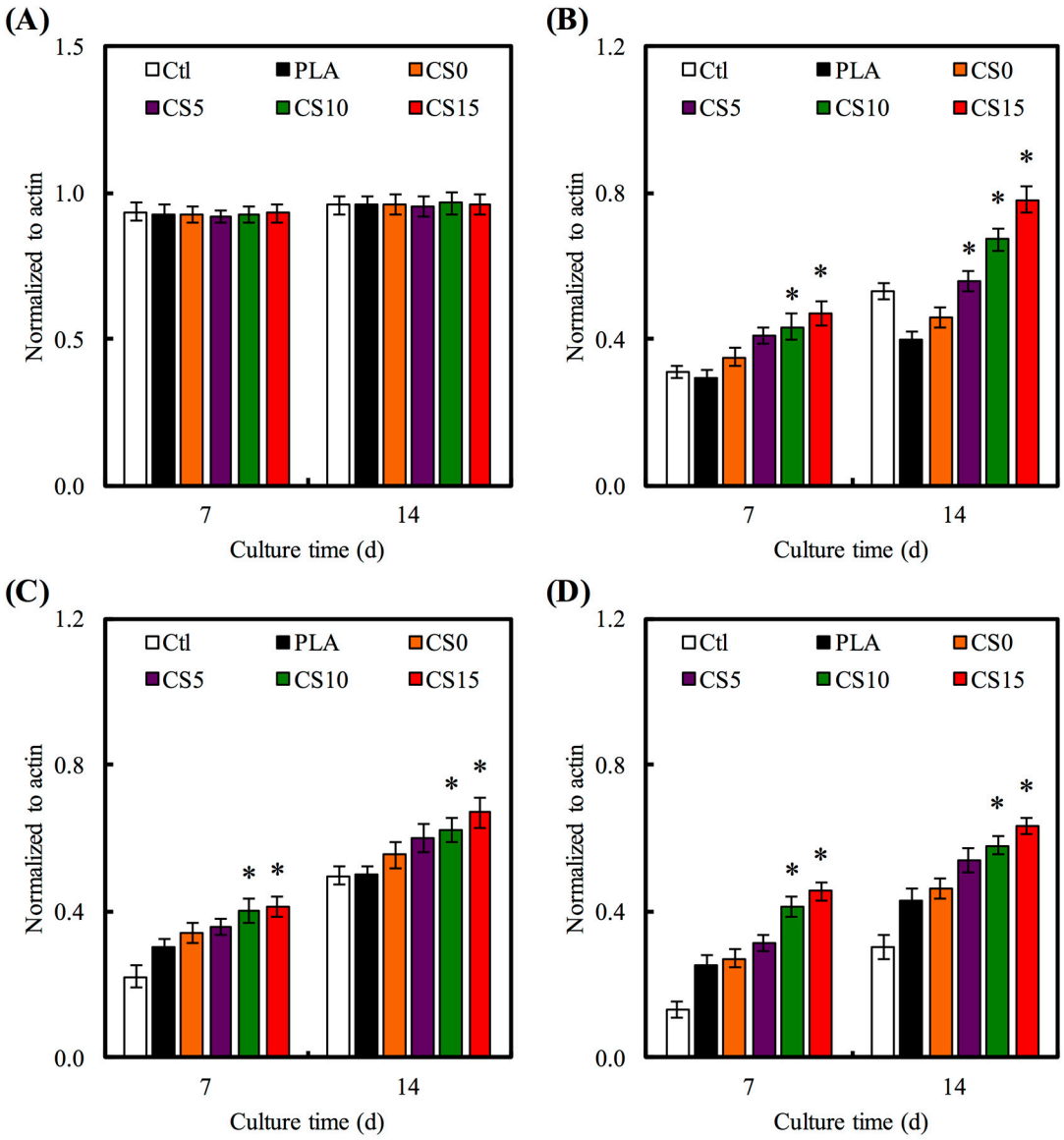

Fig. 11